

EEG-FM-Bench: A Comprehensive Benchmark for the Systematic Evaluation of EEG Foundation Models

Wei Xiong, Jiangtong Li, Jie Li, Kun Zhu

Tongji University

{xw1216, jiangtongli}@tongji.edu.cn

Abstract

Electroencephalography (EEG) foundation models are poised to significantly advance brain signal analysis by learning robust representations from large-scale, unlabeled datasets. However, their rapid proliferation has outpaced the development of standardized evaluation benchmarks, which complicates direct model comparisons and hinders systematic scientific progress. This fragmentation fosters scientific inefficiency and obscures genuine architectural advancements. To address this critical gap, we introduce EEG-FM-Bench, the first comprehensive benchmark for the systematic and standardized evaluation of EEG foundation models (EEG-FMs). Our contributions are threefold: (1) we curate a diverse suite of downstream tasks and datasets from canonical EEG paradigms, implementing standardized processing and evaluation protocols within a unified open-source framework; (2) we benchmark prominent state-of-the-art foundation models to establish comprehensive baseline results for a clear comparison of the current landscape; (3) we perform qualitative analyses of the learned representations to provide insights into model behavior and inform future architectural design. Through extensive experiments, we find that fine-grained spatio-temporal feature interaction, multi-task unified training and neuropsychological priors would contribute to enhancing model performance and generalization capabilities. By offering a unified platform for fair comparison and reproducible research, EEG-FM-Bench seeks to catalyze progress and guide the community toward the development of more robust and generalizable EEG-FMs. Code is released at <https://github.com/xw1216/EEG-FM-Bench>.

1 Introduction

EEG is a cornerstone of modern neuroscience and clinical practice. Its high temporal resolution, combined with its non-invasive nature and relative affordability, makes it an indispensable tool for investigating brain dynamics across a spectrum of contexts, including cognition, emotion, and neurological pathology (Ramantani, Maillard, and Koessler 2016). The success of large-scale, pre-trained foundation models in other domains such as computer vision (CV) (Radford et al. 2021) and natural language processing (NLP) (Devlin et al. 2019) has opened a new frontier in brain decoding, where general-purpose AI systems offer the potential for an unprecedented understanding of neural signals by learning robust representations from vast, unlabeled datasets. This potential has catalyzed the emergence

of EEG foundation models (EEG-FM) (Jiang, Zhao, and Lu 2024). These models are designed to address the canonical challenges that have long hindered progress in EEG analysis, *i.e.*, high inter-subject and intra-subject variability, substantial data variations across experimental paradigms, and the prohibitive cost of acquiring large-scale, expertly annotated datasets (Rashid et al. 2020). Early works adapt architectures from other domains, such as BENDR (Kostas, Aroca-Ouellette, and Rudzicz 2021), while subsequent innovations focus on developing architectures and pre-training strategies tailored to the unique characteristics of EEG, exemplified by models such as CBraMod (Wang et al. 2024b).

Despite the rapid progress of these foundation models, their evaluation methods remain fragmented. Models are frequently assessed on disparate downstream tasks, often employing inconsistent datasets, preprocessing pipelines, and evaluation strategies (Lai et al. 2025). This lack of standardization precludes direct and fair comparisons between competing architectures, hindering systematic progress and obscuring the true state-of-the-art (SOTA). Therefore, the community lacks a unified and comprehensive benchmark. *In EEG domain, this absence of a standard fosters scientific inefficiency and complicates the ability to distinguish genuine algorithmic advances from overfitting to specific datasets.*

To address this critical gap, we introduce **EEG-FM-Bench**, the first comprehensive benchmark for the systematic and standardized evaluation of EEG-FM. Our benchmark provides a diverse suite of curated tasks, standardized data processing pipelines, and robust evaluation protocols. These components are integrated within a unified open-source codebase to ensure reproducible research and fair comparisons. In detail, EEG-FM-Bench includes 14 datasets across 10 common paradigms, including motor imagery, sleep staging, emotion recognition, seizure detection, and Alzheimer’s Disease classification, among others. The benchmark employs three distinct fine-tuning strategies to assess pre-training quality, architecture design, and downstream generalization: *frozen backbone single-task fine-tuning*, *full-parameter single-task fine-tuning*, and *full-parameter multi-task fine-tuning*. This comprehensive task design enables a robust evaluation of the core ability of EEG-FM to generalize across diverse neurological contexts.

Our experiments evaluate five publicly available, pre-trained EEG-FM: BIOT (Yang, Westover, and Sun 2023),

BENDR (Kostas, Aroca-Ouellette, and Rudzicz 2021), LaBraM (Jiang, Zhao, and Lu 2024), EEGPT (Wang et al. 2024a), and CBraMod (Wang et al. 2024b). Our comprehensive evaluation and qualitative analyses on EEG-FM-Bench reveals several key findings: (1) A critical generalization gap emerges when using a frozen backbone, revealing that pre-trained representations often fail to transfer effectively to novel tasks; (2) A model’s capacity for cross-paradigm generalization appears contingent on its ability to capture fine-grained spatio-temporal interactions in architectural design; (3) Multi-task learning acts as a powerful catalyst for knowledge sharing, unlocking performance gains for underperforming models that are not achievable in single-task settings; (4) The choice of data processing pipelines and partitioning strategies introduces a major source of variability that critically influences model performance and benchmark outcomes; (5) Dominant pre-training objectives like masked signal reconstruction may be suboptimal, incentivizing models to learn low-level features for signal “inpainting”. These findings suggest that future progress hinges on integrating neuro-physiological priors, adapting with different electrode-configuration, and embracing multi-task learning. The primary contributions of this work are as followed:

- We introduce **EEG-FM-Bench**, the first comprehensive benchmark for EEG-FM, providing a unified open-source framework with diverse tasks and standardized protocols for end-to-end evaluation.
- We conduct a large-scale empirical study on SOTA EEG-FMs, establishing extensive baselines to provide a comparative analysis of their performance and generalization across multiple fine-tuning strategies.
- We perform qualitative analyses of the learned representations using visualization techniques such as t-SNE (Maaten and Hinton 2008) and Integrated Gradients (Sundararajan, Taly, and Yan 2017) to elucidate effective architectural principles and guide future design.

2 Related Work

2.1 EEG Foundation Models

Early efforts adapted techniques from other fields, for instance, BENDR (Kostas, Aroca-Ouellette, and Rudzicz 2021) applied contrastive learning from speech model, while many others focused on masked signal modeling. These include BrainBERT (Wang et al. 2023), which operates on EEG spectrograms, and models like EEG2Rep (Mohammadi Foumani et al. 2024) and Brant (Zhang et al. 2023) that perform masking in the latent space. A parallel line of innovation has focused on input tokenization. BIOT (Yang, Westover, and Sun 2023) introduced channel-independent methods for variable inputs, while both LaBraM (Jiang, Zhao, and Lu 2024) and EEGFormer (Wan et al. 2023) developed vector-quantized approaches for raw and frequency-domain signals. Architectural advancements are also prominent, introducing spatio-temporal alignment (EEGPT (Wang et al. 2024a)), criss-cross attention (CBraMod (Wang et al. 2024b)), and cross-scale architecture (CSBrain (Zhou et al. 2025)). Furthermore, some models expand the data by

combining scalp with intracranial EEG (Brant-2 (Yuan et al. 2024)) or targeting specific clinical challenges like Alzheimer’s disease (LEAD (Wang et al. 2025)). This rapid, multi-faceted evolution makes fair comparison between approaches nearly impossible, underscoring the critical need for standardized benchmarks to unify and guide the field.

2.2 EEG Benchmarks

Progress in AI has historically been driven by large-scale, standardized benchmarks such as ImageNet (Deng et al. 2009) in CV and GLUE (Wang et al. 2018) in NLP. In contrast, the BCI and broader EEG analysis communities have long contended with a reproducibility crisis, partly due to a lack of such unifying standards. Pioneering efforts, including a series of BCI competitions, have made significant contributions by providing public datasets and standardized evaluation metrics. More recent competitions continue this trend, with BEETL (Wei et al. 2022) highlighting transfer learning challenges and the EEG Foundation Challenge (Aristimunha et al. 2025) focusing on cross-subject cognitive tasks. MOABB (Jayaram and Barachant 2018) offers an open-source platform for evaluation, yet their scope is limited to specific paradigms such as motor imagery, SSVEP, and P300. Furthermore, numerous benchmarks have been developed for highly specific tasks or model classes, including denoising (EEGdenoiseNet (Zhang et al. 2021)), emotion recognition (LibEER (Liu et al. 2024)), Parkinson’s diagnosis (Avola et al. 2025), and the evaluation of specific architectures like GNNs (GNN4EEG (Zhang et al. 2024)). While these specialized benchmarks are valuable, a comprehensive benchmark designed for general-purpose EEG-FMs remains notably absent. Such a resource is critical for ensuring reproducible science and providing a fair basis for comparing methodological innovations.

3 Benchmark Pipeline

To ensure fair and reproducible comparisons, EEG-FM-Bench integrates a complete workflow encompassing task curation, data processing, model fine-tuning, and evaluation. This entire workflow is implemented as a modular and automated open-source framework, which provides a unified platform for future research. Figure 1 provides an overview of pipeline of EEG-FM-Bench. The data module converts raw EEG data into a more efficient file format and provides standardized preprocessing protocols for numerous datasets. The evaluation strategy module provides a flexible interface and configuration-friendly system to ensure compatibility with existing EEG-FMs, permitting them to be easily evaluated on EEG datasets and fine-tuning strategies. The analysis module provides comprehensive analysis of both quantitative and qualitative aspects (t-SNE (Maaten and Hinton 2008) for feature discrimination and Integ-Grads (Sundararajan, Taly, and Yan 2017) for decision basis).

3.1 Data

Task and Dataset Curation. Our benchmark includes a carefully curated suite of 14 publicly available datasets, spanning 10 of the most canonical EEG paradigms,

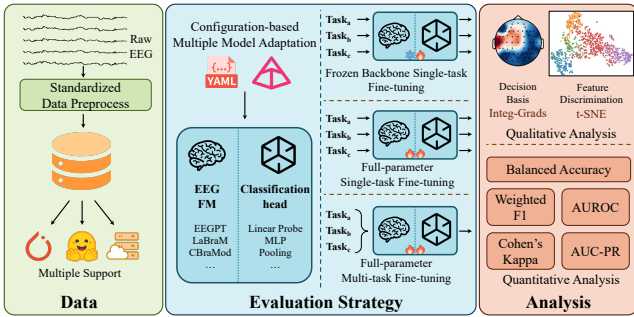


Figure 1: The pipeline of EEG-FM-Bench. **Data:** We collect 14 public datasets, spanning 10 canonical EEG paradigms along with a standardized data preprocessing to support different utilization. **Evaluation Strategy:** We separate the optimization into pretrained EEG-FMs and downstream decoder, and design a configuration-based framework with three fine-tuning strategies to evaluate different EEG-FMs. **Analysis:** We provide comprehensive analysis to evaluate the EEG-FMs from both quantitative and qualitative aspects.

including motor imagery (BCIC-2a, PhysioMI, Mimul-11), emotion recognition (SEED, SEED-V, SEED-VII), sleep stage classification (HMC), seizure detection (Siena), mental stress assessment (Workload), abnormal detection (TUAB), event type classification (TUEV), visual target detection (Things-EEG-2), Alzheimer’s Disease recognition (ADFTD) and slowing event classification (TUSL) (see Appendix for a full summary). By integrating these diverse and challenging datasets, EEG-FM-Bench functions not merely as a tool for ranking models, but as a diagnostic instrument for identifying their specific architectural and representational weaknesses. Our framework also provides an extensible API, allowing for integration of custom datasets and user-defined data assembly configurations.

Standardized Data Processing Inconsistent data processing represents a major source of variability in EEG research. To mitigate this issue, we implement a standardized preprocessing pipeline applied uniformly across all datasets. This pipeline comprises the following sequential steps:

- 1. Selection:** Data is selected based on specified event markers and a predefined set of channels.
- 2. Filtering:** A band-pass filter (0.1-128 Hz) and a notch filter (50 or 60 Hz) are applied to remove noise while maximally preserving signal information.
- 3. Resampling:** Signals are downsampled to 256 Hz to standardize temporal resolution and reduce computational load.
- 4. Segmentation:** Continuous data is segmented into fixed-length windows (e.g., 4-second trial), which are assigned to designated data splits according to task-specific rules.
- 5. Formatting:** Processed samples are converted into efficient file formats (“Parquet” for compressed storage, and “Arrow” for accelerated loading and computation).

3.2 Evaluation Strategy

We evaluate pre-trained EEG-FM using three distinct fine-tuning strategies to assess different aspects of their learned

representations and adaptability. For each strategy, a MLP with average pooling as classifier is appended to the models.

- **Frozen Backbone Single-task Fine-tuning:** Under this strategy, the weights of the pre-trained backbone are kept frozen, and only the parameters of the newly added classification head are trained. This approach evaluates the intrinsic quality and linear separability of the learned representations, assessing their “out-of-the-box” utility without task-specific adaptation.
- **Full-parameter Single-task Fine-tuning:** In this approach, the parameters of the entire model, including the pre-trained backbone and the classification head, are fine-tuned on a specific downstream task. This protocol assesses the model’s capacity to adapt its pre-trained features to the specific characteristics of a new task.
- **Full-parameter Multi-task Fine-tuning:** To investigate knowledge sharing and broad generalization, we also implement a multi-task learning approach. Using a specially designed distributed resampler, the model is simultaneously fine-tuned on a composite dataset comprising all curated tasks. This strategy evaluates a model’s ability to leverage information across multiple paradigms to enhance its performance on individual tasks.

3.3 Analysis

We perform quantitative experiments to provide a comprehensive analysis of various EEG-FMs, evaluating how different model designs and fine-tuning strategies affect their classification performance. Moreover, we provide a qualitative analysis using t-SNE and Integ-Grads visualizations to reveal the feature separability and decision-making basis of these models. To address the class imbalance in EEG tasks, we adopt the following metrics for comparison:

- * **Balanced Accuracy:** The arithmetic mean of recall across all classes. This metric mitigates the impact of imbalanced distributions and is highly effective for datasets with significant class disparities.
- * **Weighted F1:** The harmonic mean of precision and recall, where scores are weighted by the support of each class. This approach accounts for class imbalance by giving more weight to larger classes.
- * **AUROC:** The Area Under Receiver Operating Characteristic curve, reflecting the ability of models to discriminate between classes across all decision thresholds.
- * **AUC-PR:** The Area Under the Precision-Recall curve, a metric that is particularly informative for evaluating performance on datasets with significant class imbalance.
- * **Cohen’s Kappa:** A statistic that measures the level of agreement between predicted and true labels while correcting for agreement that could occur by chance. It is well-suited for multi-class classification.

Within our benchmark, AUROC and AUC-PR are used for binary classification tasks, while Cohen’s Kappa and Weighted F1 are applied to multi-class problems. These metrics provide a comprehensive framework for evaluating model performance under class imbalance.

Model	Metrics	SEED	PhysioMI	Workload	TUEV	TUAB	HMC	Siena
BENDR	B-Acc	33.33 \pm 0.00	25.00 \pm 0.00	50.00 \pm 0.00	16.67 \pm 0.00	66.59 \pm 2.46	20.00 \pm 0.00	50.00 \pm 0.00
	F1/AUROC	17.65 \pm 0.00	10.05 \pm 0.01	50.08 \pm 1.90	44.05 \pm 0.00	73.29 \pm 0.95	19.48 \pm 0.00	49.88 \pm 1.43
	Kappa/AUCPR	0.00 \pm 0.00	0.00 \pm 0.00	29.56 \pm 0.77	0.00 \pm 0.00	67.32 \pm 0.85	0.00 \pm 0.00	98.88 \pm 0.03
BIOT	B-Acc	61.26 \pm 1.18	27.21 \pm 0.20	56.66\pm1.96	43.69 \pm 2.13	77.98\pm0.75	65.61\pm2.53	66.21 \pm 0.01
	F1/AUROC	61.22\pm1.04	26.02 \pm 0.62	85.68\pm3.70	70.54 \pm 1.15	85.90 \pm 0.80	67.53\pm1.90	66.67 \pm 5.63
	Kappa/AUCPR	42.15 \pm 1.67	2.95 \pm 0.27	70.11\pm4.49	53.09 \pm 1.00	85.68 \pm 1.41	59.19\pm1.89	98.50 \pm 0.35
LaBraM	B-Acc	35.37 \pm 0.94	25.87 \pm 0.65	50.00 \pm 0.00	31.48 \pm 5.27	60.40 \pm 4.64	33.83 \pm 2.10	50.00 \pm 0.00
	F1/AUROC	26.03 \pm 2.62	16.33 \pm 1.60	58.47 \pm 7.29	61.17 \pm 3.54	74.98 \pm 1.65	35.89 \pm 0.88	53.73 \pm 2.28
	Kappa/AUCPR	5.94 \pm 2.68	1.16 \pm 0.87	37.66 \pm 7.62	35.57 \pm 7.81	73.73 \pm 1.49	20.32 \pm 1.77	99.09 \pm 0.07
EEGPT	B-Acc	61.80\pm0.65	39.90\pm1.39	52.98 \pm 4.22	49.83\pm9.60	76.64 \pm 1.04	55.61 \pm 2.81	69.58\pm4.12
	F1/AUROC	60.41 \pm 1.07	39.51\pm1.92	75.19 \pm 0.79	75.99\pm5.48	87.43\pm0.33	56.49 \pm 1.41	92.20\pm1.98
	Kappa/AUCPR	42.89\pm0.97	19.87\pm1.84	49.23 \pm 0.69	62.22\pm9.38	87.47\pm0.74	46.36 \pm 2.48	99.84\pm0.03
CBraMod	B-Acc	34.09 \pm 0.14	25.33 \pm 0.43	50.00 \pm 0.00	21.06 \pm 0.22	54.73 \pm 1.24	22.29 \pm 0.28	67.89 \pm 2.93
	F1/AUROC	18.06 \pm 0.57	22.42 \pm 1.15	61.64 \pm 0.14	51.72 \pm 0.31	58.16 \pm 1.06	14.00 \pm 0.74	85.71 \pm 0.06
	Kappa/AUCPR	1.11 \pm 0.20	0.63 \pm 0.38	41.46 \pm 0.33	14.93 \pm 0.94	54.32 \pm 0.88	1.88 \pm 0.39	99.50 \pm 0.04

Table 1: Performance comparison on 7 BCI tasks under frozen fine-tuning strategy. Siena, Workload and TUAB datasets use AUROC and AUCPR as their supplement metrics. Others use weighted F1 and Cohen’s Kappa.

4 Experiment

4.1 Experiment Setup

All models are evaluated within the EEG-FM-Bench framework. For each experiment, a MLP is appended to the EEG-FM for classification. All reported results are the mean and standard deviation in five runs with different random seeds to ensure statistical robustness. **More details about the experiment setup are in Appendix.**

4.2 Quantitative Results

The results of our experiments are summarized in Tables 1, 2, and 3, each corresponding to a fine-tuning strategy. **Due to the space limitation of main submission, quantitative results on seven other EEG datasets are in Appendix.**

* **Frozen Backbone Single-Task Fine-tuning - Generalization Gap.** This evaluation protocol freezes the pre-trained EEG-FMs and trains a linear classifier with activation, directly probing the out-of-the-box utility and linear separability of the learned representations. The results, presented in Table 1, are revealing. A catastrophic performance collapse is observed across all models and nearly all tasks. Many models perform only slightly above chance level. For example, on the 3-class SEED dataset, BENDR only achieves a Balanced Accuracy of 33.33 ± 0.00 , equivalent to random guessing. This exposes a critical generalization gap: the representations learned during pre-training are not sufficiently abstract or linearly separable to be effective for downstream tasks without substantial, task-specific adaptation of the entire network. This widespread failure suggests that current pre-training objectives, which are predominantly based on masked signal reconstruction, may incentivize models to learn low-level features sufficient for “inpainting” the signal rather than high-level semantic representations of the underlying neural code. While some models like BIOT and EEGPT show slightly better resilience on certain tasks (e.g., BIOT achieves a B-Acc of 77.98 ± 0.75 on TUAB), the overarching conclusion is that the utility of current EEG-FMs as simple, off-the-shelf feature extractors

is severely limited. The pre-trained weights serve as a good initialization point for full fine-tuning but do not, in their raw form, constitute a universally powerful feature space.

* **Full-Parameter Single-Task Fine-tuning - Model Adaptability.** This full fine-tuning strategy, where all model parameters are updated for each downstream task, is designed to measure the maximal adaptive performance of each EEG-FM (results are detailed in Table 2). Results reveal a competitive but varied performance landscape, with no single model achieving state-of-the-art performance across all tasks. This heterogeneity highlights the task-specific strengths and weaknesses of current architectures. Notably, CBraMod and EEGPT emerge as frequent top performers. **CBraMod** excels on mental stress (Workload, B-Acc: 71.94 ± 0.60) and emotion recognition (SEED, B-Acc: 70.83 ± 0.28), likely due to its criss-cross attention mechanism that disentangles spatial and temporal dependencies for precise motor cortex modeling. Meanwhile, **EEGPT** is good at emotion recognition (SEED, B-Acc: 69.81 ± 1.45) and excels on artifact detection (TUEV, B-Acc: 66.86 ± 2.54). Its novel dual self-supervised pre-training, which aligns latent features instead of reconstructing the raw signal, may yield more robust representations less susceptible to the low signal-to-noise ratio of these tasks. Moreover, **LaBraM**, pre-trained on approx. 2,500 hours of EEG data, shows consistently strong performance across many tasks (e.g., PhysioMI, B-Acc: 57.27 ± 0.26). Its vector-quantized neural tokenizer likely provides a rich and versatile codebook of neural patterns. However, its failure to consistently outperform models with less pre-training data (EEGPT) suggests vector quantization may limit its representational capacity for certain fine-grained EEG signals. **BIOT**’s main contribution is its channel-independent tokenization scheme, enabling cross-dataset learning. While a significant engineering achievement for data harmonization, its performance is moderate (e.g., PhysioMI, B-Acc: 27.38 ± 0.35), suggesting its generic transformer backbone is less effective than specialized designs in capturing spatio-temporal interactions. **BENDR**, an early EEG-FM from speech processing,

Model	Metrics	SEED	PhysioMI	Workload	TUEV	TUAB	HMC	Siena
BENDR	B-Acc	59.50 \pm 0.42	47.78 \pm 0.28	50.00 \pm 0.00	65.53 \pm 2.40	82.72\pm0.12	72.63\pm0.13	74.93 \pm 1.76
	F1/AUROC	58.88 \pm 0.98	42.72 \pm 8.93	52.36 \pm 1.25	80.95 \pm 2.18	89.52\pm0.14	73.67\pm0.53	90.90 \pm 3.60
	Kappa/AUCPR	39.42 \pm 0.64	36.48 \pm 8.47	30.70 \pm 0.55	66.62 \pm 4.07	90.68\pm0.13	65.86\pm0.70	99.81 \pm 0.08
BIOT	B-Acc	63.87 \pm 1.77	27.38 \pm 0.35	63.98 \pm 0.66	57.07 \pm 4.29	79.52 \pm 0.59	71.01 \pm 0.07	64.93 \pm 2.70
	F1/AUROC	63.12 \pm 1.94	26.01 \pm 0.62	77.68 \pm 1.62	74.34 \pm 4.00	88.27 \pm 0.16	72.27 \pm 0.11	70.17 \pm 2.73
	Kappa/AUCPR	45.99 \pm 2.67	3.18 \pm 0.46	69.30\pm2.27	39.55 \pm 24.15	88.45 \pm 0.07	64.40 \pm 0.35	98.93 \pm 0.20
LaBraM	B-Acc	61.59 \pm 1.71	57.27\pm0.26	55.82 \pm 1.72	59.58 \pm 4.31	79.50 \pm 0.81	69.87 \pm 0.10	59.11 \pm 4.05
	F1/AUROC	60.30 \pm 1.60	57.29\pm0.25	78.19 \pm 0.48	77.72 \pm 3.25	86.91 \pm 0.51	70.92 \pm 0.23	81.76 \pm 1.97
	Kappa/AUCPR	43.28 \pm 2.48	43.00\pm0.35	59.36 \pm 1.26	64.06 \pm 5.03	83.86 \pm 1.96	63.10 \pm 0.31	99.65 \pm 0.07
EEGPT	B-Acc	69.81 \pm 0.45	54.16 \pm 0.18	62.31 \pm 3.98	66.86\pm2.54	78.66 \pm 0.24	69.67 \pm 1.24	76.25 \pm 1.02
	F1/AUROC	69.49 \pm 0.62	53.27 \pm 0.92	70.46 \pm 4.00	83.95\pm0.14	87.52 \pm 1.01	73.03 \pm 0.32	92.08 \pm 1.15
	Kappa/AUCPR	54.89 \pm 0.67	38.04 \pm 1.08	48.13 \pm 6.90	74.45\pm0.09	86.94 \pm 2.15	64.64 \pm 0.92	99.81 \pm 0.02
CBraMod	B-Acc	70.83\pm0.28	56.74 \pm 0.36	71.94\pm0.60	62.22 \pm 2.49	78.31 \pm 0.46	71.48 \pm 0.40	80.64\pm1.40
	F1/AUROC	80.48\pm0.16	56.74 \pm 0.39	81.63\pm1.63	76.78 \pm 2.10	88.02 \pm 1.08	72.76 \pm 0.55	93.86\pm0.25
	Kappa/AUCPR	56.63\pm0.42	42.31 \pm 0.48	59.73 \pm 1.79	61.42 \pm 2.74	88.24 \pm 1.09	64.86 \pm 0.41	99.87\pm0.01

Table 2: Performance comparison on 7 BCI tasks under separate fine-tuning strategy. Siena, Workload and TUAB datasets use AUROC and AUCPR as their supplement metrics. Others use weighted F1 and Cohen’s Kappa.

generally lags behind recent counterparts in complicated cognition tasks. The performance gap highlights the rapid progress of this field and the need for architectures tailored to unique characteristics of EEG.

*** Full-Parameter Multi-Task Fine-tuning - Knowledge Sharing.** In this setup, models are fine-tuned simultaneously on a composite dataset comprising all 14 tasks, testing their ability to leverage shared knowledge. The results, presented in Table 3, demonstrate the powerful effect of this paradigm. Comparing the multi-task results (Table 3) with the single-task results (Table 2), a clear trend emerges: multi-task learning acts as a potent catalyst for performance, particularly for the models that are not top-tier in the single-task setting. For instance, the performance of BIOT on Workload sees a remarkable improvement from a Balanced Accuracy of 63.98 ± 0.66 to 71.37 ± 2.19 . Similarly, the performance of BENDR on the same task jumps from 50.00 ± 0.00 to 63.32 ± 2.29 . This suggests that despite the apparent diversity of the tasks, there exists a shared underlying structure in EEG signals that the models can exploit. The multi-task setting effectively increases the volume and diversity of the training data, acting as a strong regularizer that prevents overfitting to the idiosyncrasies of any single dataset and forces the models to learn more generalizable neural features. However, we also observe cases of negative transfer, where performance on certain datasets like PhysioMI consistently decreases. The asymmetric conditional positional encoding, particularly designed for one dataset, might hinder CBraMod from benefiting from unified training. This suggests that the underlying neural patterns for motor imagery and structure designed for specific input may differ significantly from those of the other tasks, leading to a degree of destructive interference during joint training.

4.3 Qualitative Analysis

To gain deeper insight into model behavior under the unified fine-tuning strategy, we conduct a qualitative analysis. Results are shown in Figure 2. First, we use t-SNE to visualize feature embeddings from the SEED and Workload

test sets. High-performing models, such as CBraMod and EEGPT, produce well-defined and clearly separated clusters for different classes. In contrast, the embeddings from BENDR and BIOT show significant overlap and poor separation. This visualization illustrates the difficulty these models have in learning task-relevant features, a finding that aligns with their lower accuracy scores.

Second, we generate saliency maps using integrated gradients to investigate which EEG channels the models utilize for decision-making. The analysis reveals that the more successful models learn to focus on neurophysiologically relevant brain regions. For instance, for emotion recognition, CBraMod and EEGPT consistently assign higher importance to channels over the prefrontal and temporal lobes, while for the mental workload task, they prioritize channels in the frontal and parietal regions. This suggests that these models learn meaningful and generalizable patterns from the EEG signals. This comparative qualitative analysis demonstrates that observed performance differences are directly linked to the interpretability of the learned representations. The best-performing models excel not only in accuracy but also in their ability to form distinct feature spaces and identify physiologically relevant patterns of brain activity.

5 Further Discussion

In this section, we synthesize our benchmark results and the broader literature to discuss core principles of data handling and model design for EEG-FMs, aiming to provide actionable recommendations for the community.

5.1 Dataset

Our experiments demonstrate that data processing and partitioning strategies are not logistical preliminaries but are critical for model performance and benchmark validity.

*** Standardized Preprocessing.** The current fragmented landscape of EEG preprocessing pipelines hinders direct model comparisons and the development of general-purpose foundation models. By implementing a unified, minimalist pipeline (band-pass/notch filtering, resampling, segmen-

Model	Metrics	SEED	PhysioMI	Workload	TUEV	TUAB	HMC	Siena
BENDR	B-Acc	60.82 \pm 0.19	44.77 \pm 0.31	63.32 \pm 2.29	67.46 \pm 2.59	84.05\pm0.26	70.21 \pm 0.72	78.96 \pm 3.08
	F1/AUROC	60.84 \pm 0.20	44.63 \pm 0.03	74.09 \pm 1.04	84.56 \pm 1.82	90.38\pm0.27	72.44 \pm 0.65	91.31 \pm 4.74
	Kappa/AUCPR	41.59 \pm 0.16	26.33 \pm 0.40	54.78 \pm 1.84	72.85 \pm 2.87	91.58\pm0.15	64.57 \pm 0.90	99.81 \pm 0.11
BIOT	B-Acc	62.62 \pm 0.94	29.04 \pm 0.24	71.37 \pm 2.19	57.81 \pm 1.30	80.85 \pm 0.36	71.45 \pm 1.05	64.07 \pm 1.56
	F1/AUROC	62.57 \pm 0.87	28.81 \pm 0.29	72.43 \pm 1.94	76.77 \pm 0.42	88.67 \pm 0.62	72.89\pm0.34	78.06 \pm 7.16
	Kappa/AUCPR	44.11 \pm 1.42	5.39 \pm 0.32	69.52 \pm 0.23	63.24 \pm 0.57	89.01 \pm 0.47	64.89 \pm 0.71	99.26 \pm 0.39
LaBraM	B-Acc	67.71 \pm 0.55	43.19 \pm 1.03	61.24 \pm 0.64	67.34 \pm 2.06	79.36 \pm 0.31	71.63\pm1.04	71.99 \pm 1.78
	F1/AUROC	68.11 \pm 0.66	42.38 \pm 1.15	67.84 \pm 4.38	83.14 \pm 3.12	85.81 \pm 0.94	72.28 \pm 1.08	87.09 \pm 3.70
	Kappa/AUCPR	52.22 \pm 0.83	24.25 \pm 1.37	54.94 \pm 3.49	72.47 \pm 5.02	83.83 \pm 1.78	65.22\pm1.23	99.76 \pm 0.08
EEGPT	B-Acc	70.70 \pm 0.88	50.52\pm0.80	72.66\pm0.90	70.85\pm1.16	79.76 \pm 0.59	71.30 \pm 0.91	83.28\pm1.56
	F1/AUROC	70.34 \pm 1.17	50.26\pm0.76	81.16\pm3.42	86.35\pm0.47	88.48 \pm 0.18	72.46 \pm 0.96	93.44\pm0.12
	Kappa/AUCPR	56.23 \pm 1.32	34.00\pm1.06	64.30 \pm 6.48	77.69\pm1.06	88.18 \pm 0.38	64.86 \pm 0.77	99.86\pm0.00
CBraMod	B-Acc	72.25\pm1.90	31.15 \pm 2.27	65.95 \pm 2.50	69.41 \pm 1.86	80.49 \pm 0.11	68.31 \pm 1.63	82.75 \pm 2.10
	F1/AUROC	72.90\pm1.63	28.83 \pm 3.48	80.68 \pm 3.81	83.44 \pm 0.31	90.18 \pm 0.48	69.66 \pm 0.48	92.03 \pm 1.90
	Kappa/AUCPR	58.68\pm2.91	8.21 \pm 3.03	70.22\pm3.41	72.02 \pm 0.65	90.03 \pm 0.55	42.73 \pm 25.88	99.83 \pm 0.04

Table 3: Performance comparison on 7 BCI tasks under unified fine-tuning strategy. Siena, Workload and TUAB datasets use AUROC and AUCPR as their supplement metrics. Others use weighted F1 and Cohen’s Kappa.

tation), our benchmark ensures performance differences reflect architectural innovations and pre-training quality, not bespoke feature engineering. This standardization is crucial for scalability, reducing data curation overhead, and facilitating the creation of large, plug-and-play EEG corpora, akin to those in NLP and CV, thereby accelerating research.

* **Dataset Selection.** The philosophy behind our downstream task selection, probing specific, generalizable capabilities, should be extended to the curation of large-scale pre-training datasets. We advocate for a cautious approach, prioritizing datasets that represent canonical neural paradigms. The inclusion of datasets that rely on highly specialized, hand-crafted features or exist in unique, non-generalizable feature spaces may introduce “negative transfer”, compelling the model to learn idiosyncratic patterns that are detrimental to its generalization capacity. The goal should be to curate a diverse and foundational corpus that encourages the learning of universal neural primitives.

* **Subject-Independent Splitting.** Our benchmark rigorously enforces subject-independent training, validation, and testing splits, which is crucial for evaluating real-world EEG model performance given significant inter-subject variability. Although emotion recognition task still employs it, subject-dependent splits lead to artificially inflated metrics that do not reflect generalizability. To foster rigor and reproducibility in future EEG-FM research, we propose a standardized protocol: datasets must be partitioned at the subject level, ensuring no identity overlap, with class balance maintained within splits. Furthermore, all results should be reported as the mean and standard deviation over multiple runs with different random seeds, enabling reliable distinction between true algorithmic advances and overfitting.

5.2 Architectural Design

Our analysis of the five benchmarked models highlights a clear evolutionary path in their design: a distinct shift from adapting general-purpose sequence models to building highly specialized, neuro-informed architectures.

* **Signal Tokenization.** Tokenization, the conversion of

continuous EEG signals into discrete patches, is a critical design choice in EEG analysis. Early models like BENDR used convolutional encoders, while BIOT introduced channel-independent patching to handle variable channel counts. LaBraM advanced this process by using a learned tokenizer to create a discrete codebook of EEG “words”. More recent models like CBraMod integrate domain knowledge directly into tokenization by extracting features from both the time and frequency domains. This evolution underscores the role of the tokenizer in embedding inductive biases, demonstrating that encoding neuroscientific priors (*e.g.*, brain activities or brain networks) is more effective than relying on generic backbones in the future.

* **Spatial Dependency.** Effectively modeling inter-channel spatial relationships is a crucial challenge. Models like BIOT and EEGPT used learnable positional embeddings, whereas more advanced models employ refined mechanisms to represent spatial structure. CBraMod, for instance, uses a criss-cross attention mechanism to explicitly compute heterogeneous dependencies across both space and time. This trend suggests a convergence with geometric deep learning, which models the functional organization of brain as a graph. Future work will likely integrate sophisticated graph representations informed by **anatomical priors or pre-computed functional connectivity matrices** to create more robust and biologically-grounded inductive biases.

* **Spatio-Temporal Correlation.** Modeling the intricate spatio-temporal evolution of neural activity is a critical challenge in EEG analysis. Standard transformer architectures, such as LaBraM and EEGPT, typically apply dense attention across all spatio-temporal tokens. This dense approach is computationally expensive and risks modeling spurious correlations, particularly given the low signal-to-noise ratio of EEG signals. Improved architectures like CBraMod use parallel attention streams to model fine-grained interactions, enabling the learning of precise spatio-temporal motifs. Future designs should prioritize the **fine-grained, multi-scale spatio-temporal interaction across brain networks** to achieve robust performance on diverse EEG paradigms.

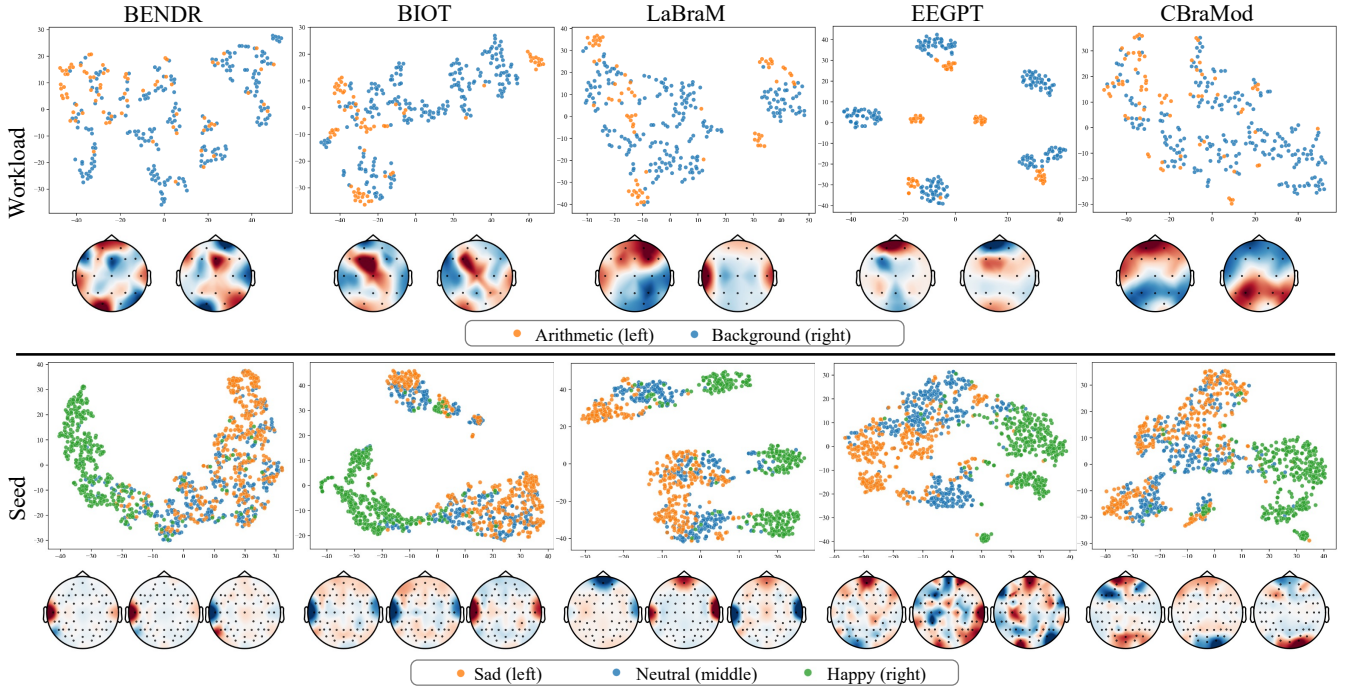


Figure 2: t-SNE and Integrated Gradients visualization for Workload (upper) and Seed (bottom) datasets.

*** Classification Head.** A surprising and critical finding is the profound impact of the classification head’s architecture: on the BCIC-2a dataset, replacing a simple classifier with a large MLP to process CBraMod’s output boosted performance by over 10%. This suggests the foundation model’s representations are not fully disentangled, as a high-capacity MLP is still needed to resolve complex spatio-temporal interactions in the final classification stage. This implies that even advanced backbones like CBraMod lack complete feature fusion, highlighting a need for terminal layers that produce more linearly separable, high-level representations.

5.3 Training Strategy

*** Beyond Masked Signal Reconstruction.** While Masked Auto-Encoding (MAE) is a popular pre-training strategy, our findings reveal its limitations for EEG. A significant “stage gap” exists between MAE’s low-level reconstruction objective and the high-level semantics required for downstream classification. Furthermore, unlike in NLP and CV, increasing pre-training data size does not yield predictable performance gains, suggesting MAE struggles to efficiently capture EEG semantics. The field needs more sophisticated self-supervised objectives, such as scaling contrastive methods to capture high-level semantics, exploring knowledge-guided objectives to generate neuro-physiological features, and utilizing dual-objective models to stabilize the training from low signal-to-noise ratio targets.

*** Multi-Task Learning** Our results (Table 3) demonstrate that multi-task learning yields significant performance gains, particularly for less specialized models such as BENDR and BIOT. This indicates substantial knowledge sharing across

diverse EEG paradigms and suggests the presence of an underlying shared statistical structure. This joint training appears to act as a powerful regularizer, fostering more robust and comprehensive internal representations of EEG signals. Therefore, integrating high-level multi-task semantic learning into the pre-training process is a promising direction for creating more versatile and powerful foundation models.

6 Conclusion and Future Perspectives

In this work, we introduce EEG-FM-Bench, the first comprehensive benchmark for EEG-FMs, establishing baselines for five SOTA models across 14 datasets and 10 paradigms within an open-source framework. We identify a major generalization gap where frozen-backbone models perform poorly, suggesting current objectives like masked reconstruction yield insufficiently abstract representations. Our findings also show that architectures incorporating EEG characteristics, such as spatio-temporal dependencies, consistently outperform generic models. Furthermore, multi-task learning is a powerful strategy that boosts performance by enabling knowledge sharing across EEG paradigms.

Based on these findings, we propose three key directions for future research. First is the need for **rethinking pre-training objectives** by moving beyond simple reconstruction toward methods that create high-level semantic representations. Second, developing **neuro-informed architectures** that explicitly model brain connectivity is essential for learning physiologically grounded representations. Finally, **embracing multi-task and multi-modal learning** by integrating complementary data, such as fMRI, is crucial for building more holistic models of brain function.

References

Alvarez-Estevez, D.; and Rijsman, R. M. 2021. Inter-database validation of a deep learning approach for automatic sleep scoring. *PLOS ONE*, 16(8): 1–27.

Aristimunha, B.; Truong, D.; Guetschel, P.; Shirazi, S. Y.; Guyon, I.; Franco, A. R.; Milham, M. P.; Dotan, A.; Makeig, S.; Gramfort, A.; et al. 2025. EEG Foundation Challenge: From Cross-Task to Cross-Subject EEG Decoding. *arXiv preprint arXiv:2506.19141*.

Avola, D.; Bernardini, A.; Crocetti, G.; Ladogana, A.; Lezoche, M.; Mancini, M.; Pannone, D.; and Ranaldi, A. 2025. Benchmarking of EEG Analysis Techniques for Parkinson’s Disease Diagnosis: A Comparison between Traditional ML Methods and Foundation DL Methods. *arXiv:2507.13716*.

Deng, J.; Dong, W.; Socher, R.; Li, L.-J.; Li, K.; and Fei-Fei, L. 2009. Imagenet: A large-scale hierarchical image database. In *2009 IEEE conference on computer vision and pattern recognition*, 248–255. Ieee.

Detti, P.; Vatti, G.; and Zabalo Manrique de Lara, G. 2020. EEG Synchronization Analysis for Seizure Prediction: A Study on Data of Noninvasive Recordings. *Processes*, 8(7).

Devlin, J.; Chang, M.-W.; Lee, K.; and Toutanova, K. 2019. BERT: Pre-training of deep bidirectional transformers for language understanding. In *NAACL*, 4171–4186.

Gifford, A. T.; Dwivedi, K.; Roig, G.; and Cichy, R. M. 2022. A large and rich EEG dataset for modeling human visual object recognition. *NeuroImage*, 264: 119754.

Gramfort, A.; Luessi, M.; Larson, E.; Engemann, D. A.; Strohmeier, D.; Brodbeck, C.; Goj, R.; Jas, M.; Brooks, T.; Parkkonen, L.; and Hämäläinen, M. 2013. MEG and EEG data analysis with MNE-Python. *Frontiers in Neuroscience*, 7.

Harati, A.; Golmohammadi, M.; Lopez, S.; Obeid, I.; and Picone, J. 2015. Improved EEG event classification using differential energy. In *SPMB*, 1–4.

Jayaram, V.; and Barachant, A. 2018. MOABB: trustworthy algorithm benchmarking for BCIs. *Journal of neural engineering*, 15(6): 066011.

Jeong, J.-H.; Cho, J.-H.; Shim, K.-H.; Kwon, B.-H.; Lee, B.-H.; Lee, D.-Y.; Lee, D.-H.; and Lee, S.-W. 2020. Multimodal signal dataset for 11 intuitive movement tasks from single upper extremity during multiple recording sessions. *GigaScience*, 9(10): giaa098.

Jiang, W.-B.; Liu, X.-H.; Zheng, W.-L.; and Lu, B.-L. 2024. Seed-vii: A multimodal dataset of six basic emotions with continuous labels for emotion recognition. *IEEE Transactions on Affective Computing*.

Jiang, W.-B.; Zhao, L.-M.; and Lu, B.-L. 2024. Large brain model for learning generic representations with tremendous EEG data in BCI. *arXiv preprint arXiv:2405.18765*.

Kostas, D.; Aroca-Ouellette, S.; and Rudzicz, F. 2021. BENDR: Using transformers and a contrastive self-supervised learning task to learn from massive amounts of EEG data. *Frontiers in Human Neuroscience*, 15: 653659.

Lai, J.; Wei, J.; Yao, L.; and Wang, Y. 2025. A Simple Review of EEG Foundation Models: Datasets, Advancements and Future Perspectives. *arXiv preprint arXiv:2504.20069*.

Liu, H.; Yang, S.; Zhang, Y.; Wang, M.; Gong, F.; Xie, C.; Liu, G.; Liu, Z.; Liu, Y.-J.; Lu, B.-L.; et al. 2024. Libeer: A comprehensive benchmark and algorithm library for eeg-based emotion recognition. *arXiv preprint arXiv:2410.09767*.

Liu, W.; Qiu, J.-L.; Zheng, W.-L.; and Lu, B.-L. 2022. Comparing Recognition Performance and Robustness of Multimodal Deep Learning Models for Multimodal Emotion Recognition. *IEEE TCDS*, 14(2): 715–729.

López, S.; Suarez, G.; Jungreis, D.; Obeid, I.; and Picone, J. 2015. Automated identification of abnormal adult EEGs. In *SPMB*, 1–5.

Maaten, L. v. d.; and Hinton, G. 2008. Visualizing data using t-SNE. *Journal of machine learning research*, 9(Nov): 2579–2605.

Miltiadous, A.; Tzimourta, K. D.; Afrantou, T.; Ioannidis, P.; Grigoriadis, N.; Tsalikakis, D. G.; Angelidis, P.; Tsipouras, M. G.; Glavas, E.; Giannakeas, N.; et al. 2023. A dataset of scalp EEG recordings of Alzheimer’s disease, frontotemporal dementia and healthy subjects from routine EEG. *Data*, 8(6): 95.

Mohammadi Foumani, N.; Mackellar, G.; Ghane, S.; Irtza, S.; Nguyen, N.; and Salehi, M. 2024. Eeg2rep: enhancing self-supervised eeg representation through informative masked inputs. In *Proceedings of the 30th ACM SIGKDD Conference on Knowledge Discovery and Data Mining*, 5544–5555.

Radford, A.; Kim, J. W.; Hallacy, C.; Ramesh, A.; Goh, G.; Agarwal, S.; Sastry, G.; Askell, A.; Mishkin, P.; Clark, J.; et al. 2021. Learning transferable visual models from natural language supervision. In *International conference on machine learning*, 8748–8763. PMLR.

Ramantani, G.; Maillard, L.; and Koessler, L. 2016. Correlation of invasive EEG and scalp EEG. *Seizure*, 41: 196–200.

Rashid, M.; Sulaiman, N.; PP Abdul Majeed, A.; Musa, R. M.; Ab. Nasir, A. F.; Bari, B. S.; and Khatun, S. 2020. Current status, challenges, and possible solutions of EEG-based brain-computer interface: a comprehensive review. *Frontiers in neurorobotics*, 14: 25.

Schalk, G.; McFarland, D.; Hinterberger, T.; Birbaumer, N.; and Wolpaw, J. 2004. BCI2000: a general-purpose brain-computer interface (BCI) system. *IEEE TBE*, 51(6): 1034–1043.

Sundararajan, M.; Taly, A.; and Yan, Q. 2017. Axiomatic attribution for deep networks. In *International conference on machine learning*, 3319–3328. PMLR.

Van Den Oord, A.; Vinyals, O.; et al. 2017. Neural discrete representation learning. In *NeurIPS*.

von Weltin, E.; Ahsan, T.; Shah, V.; Jamshed, D.; Golmohammadi, M.; Obeid, I.; and Picone, J. 2017. Electroencephalographic slowing: A primary source of error in automatic seizure detection. In *SPMB*, 1–5.

Wan, Z.; Li, M.; Liu, S.; Huang, J.; Tan, H.; and Duan, W. 2023. EEGformer: A transformer-based brain activity classification method using EEG signal. *Frontiers in neuroscience*, 17: 1148855.

Wang, A.; Singh, A.; Michael, J.; Hill, F.; Levy, O.; and Bowman, S. R. 2018. GLUE: A multi-task benchmark and analysis platform for natural language understanding. *arXiv preprint arXiv:1804.07461*.

Wang, C.; Subramaniam, V.; Yaari, A. U.; Kreiman, G.; Katz, B.; Cases, I.; and Barbu, A. 2023. BrainBERT: Self-supervised representation learning for intracranial recordings. *arXiv preprint arXiv:2302.14367*.

Wang, G.; Liu, W.; He, Y.; Xu, C.; Ma, L.; and Li, H. 2024a. Eegpt: Pretrained transformer for universal and reliable representation of eeg signals. *Advances in Neural Information Processing Systems*, 37: 39249–39280.

Wang, J.; Zhao, S.; Luo, Z.; Zhou, Y.; Jiang, H.; Li, S.; Li, T.; and Pan, G. 2024b. Cbramod: A criss-cross brain foundation model for eeg decoding. *arXiv preprint arXiv:2412.07236*.

Wang, Y.; Huang, N.; Mammone, N.; Cecchi, M.; and Zhang, X. 2025. LEAD: Large Foundation Model for EEG-Based Alzheimer’s Disease Detection. *arXiv preprint arXiv:2502.01678*.

Wei, X.; Faisal, A. A.; Grosse-Wentrup, M.; Gramfort, A.; Chevallier, S.; Jayaram, V.; Jeunet, C.; Bakas, S.; Ludwig, S.; Barmpas, K.; et al. 2022. 2021 BEETL competition: Advancing transfer learning for subject independence and heterogenous EEG data sets. In *NeurIPS 2021 Competitions and Demonstrations Track*, 205–219. PMLR.

Yang, C.; Westover, M.; and Sun, J. 2023. Biot: Biosignal transformer for cross-data learning in the wild. *Advances in Neural Information Processing Systems*, 36: 78240–78260.

Yuan, Z.; Zhang, D.; Chen, J.; Gu, G.; and Yang, Y. 2024. Brant-2: Foundation model for brain signals. *CoRR*.

Zhang, D.; Yuan, Z.; Yang, Y.; Chen, J.; Wang, J.; and Li, Y. 2023. Brant: Foundation model for intracranial neural signal. *Advances in Neural Information Processing Systems*, 36: 26304–26321.

Zhang, H.; Zhao, M.; Wei, C.; Mantini, D.; Li, Z.; and Liu, Q. 2021. EEGdenoiseNet: a benchmark dataset for deep learning solutions of EEG denoising. *Journal of Neural Engineering*, 18(5): 056057.

Zhang, K.; Ye, Z.; Ai, Q.; Xie, X.; and Liu, Y. 2024. Gnn4eeg: A benchmark and toolkit for electroencephalography classification with graph neural network. In *Companion of the 2024 on ACM International Joint Conference on Pervasive and Ubiquitous Computing*, 612–617.

Zheng, W.-L.; and Lu, B.-L. 2015. Investigating Critical Frequency Bands and Channels for EEG-Based Emotion Recognition with Deep Neural Networks. *IEEE TAMD*, 7(3): 162–175.

Zhou, Y.; Wu, J.; Ren, Z.; Yao, Z.; Lu, W.; Peng, K.; Zheng, Q.; Song, C.; Ouyang, W.; and Gou, C. 2025. CSBrain: A Cross-scale Spatiotemporal Brain Foundation Model for EEG Decoding. *arXiv preprint arXiv:2506.23075*.

Zyma, I.; Tukaev, S.; Seleznov, I.; Kiyono, K.; Popov, A.; Chernykh, M.; and Shpenkov, O. 2019. Electroencephalograms during Mental Arithmetic Task Performance. *Data*, 4(1).

This supplementary material provides additional details, analyses, and experiments to support our main findings. The contents are organized as follows:

- Appendix A and B provides detailed descriptions of the datasets used for fine-tuning, along with our complete experimental settings.
- Appendix C presents the extended experimental data on the remaining 7 datasets that are not included in the main text due to space limitations.
- Appendix D and E contains additional visualizations of the EEG signals, followed by statistical validation of models' performance.
- Appendix F concludes with a discussion of the limitations of the current work and outlines promising directions for future research.

A Datasets Description

Detailed information for the evaluation datasets is in Tab. 4:

1. Seizure Detection: Siena (Detti, Vatti, and Zabalo Manrique de Lara 2020) (binary classification with seizure or healthy);
2. Emotion Recognition: SEED (Zheng and Lu 2015) (3-class classification with sad, neutral or happy), SEED-V (Liu et al. 2022) (5-class classification with disgust, fear, sad, neutral or happy), SEED-VII (Jiang et al. 2024) (7-class classification with disgust, fear, sad, neutral, happy, anger or surprise);
3. Motor Imagery: PhysioMI (Schalk et al. 2004) (4-class classification with left fist, right fist, both fists or feet), Mimul-11 (Jeong et al. 2020) (3-class classification with reaching, grasping or twisting), BCIC-2a (Rashid et al. 2020) (4-class classification with left hand, right hand, feet or tongue);
4. Mental Stress: Workload (Zyma et al. 2019) (binary-class classification with arithmetic calculation or resting); 5) Sleep Staging: HMC (Alvarez-Estevez and Rijssman 2021) (5-class classification with wake, REM, N1, N2 or N3);
5. Anomalous Event Detection: TUEV (Harati et al. 2015) (6-class classification with spike and slow wave, generalized periodic epileptiform discharge, periodic lateralized epileptiform discharge, eye movement artifact or background);
6. Abnormal Classification: TUAB (López et al. 2015) (binary-class classification with abnormal or normal);
7. Visual Target Detection: Things-EEG-2 (Gifford et al. 2022) (binary-class classification with target or non-target);
8. Alzheimer's Disease Identification: ADFTD (Miltiadous et al. 2023) (3-class classification with Alzheimer's Disease, Frontotemporal Dementia or healthy);
9. Slowing Event Classification: TUSL (von Weltin et al. 2017) (3-class classification with seizure, slow wave or background).

B Experimental Setup

B.1 Data pre-processing

Our dataset pre-processing pipeline follows a systematic procedure to process EEG data from multiple sources, implemented using MNE-Python (Gramfort et al. 2013). The process begins by resampling the data to a uniform sampling rate of $f_s = 256$ Hz, which allows for consistent patch division. To eliminate low-frequency noise, we apply a high-pass Finite Impulse Response (FIR) filter that uses an overlap-add method, a technique chosen for its effectiveness on signals of variable or short durations. Moreover, power-line interference is suppressed using a notch filter at either 50 Hz or 60 Hz; the specific frequency is chosen by manually inspecting each dataset's power spectrum or its geographical origin. Next, the electrode layout from each dataset is standardized to a 10-10 montage, discarding any unsupported channels. The data units are then converted from micro-volts (μ V) to Volts to align with the MNE-Python standard. For optimized data management, the processed EEG signals are serialized into either the Parquet format with Zstandard compression for storage efficiency or the Arrow format to accelerate data loading and computation. The pipeline also supports large-scale distributed training by accessing datasets directly from remote storage via the S3 protocol. The entire implementation is built on parallel processing to efficiently handle the terabytes of data in the pre-training corpus.

B.2 Comparing Foundation Models

Our analysis contrasts five state-of-the-art EEG Foundation Models: BENDR (Kostas, Aroca-Ouellette, and Rudzicz 2021), BIOT (Yang, Westover, and Sun 2023), LaBraM (Jiang, Zhao, and Lu 2024), EEGPT (Wang et al. 2024a), and CBraMod (Wang et al. 2024b). BENDR (Kostas, Aroca-Ouellette, and Rudzicz 2021) employs a BERT-style objective on a large clinical EEG corpus. To manage data heterogeneity, BIOT (Yang, Westover, and Sun 2023) tokenizes different biosignals into a single, sentence-like format. LaBraM undergoes pre-training on 2,500 hours of data with VQ-VAE (Van Den Oord, Vinyals et al. 2017) modules for dual-domain (frequency/phase) mask learning. EEGPT merges dual self-supervised learning with stabilization mechanisms, and CBraMod (Wang et al. 2024b) uses criss-cross attention to capture spatial and temporal features separately in the same transformer layer, which refines its representational ability. Moreover, EEGPT's framework supports multi-task evaluation by applying different linear probes to its frozen pre-trained backbone. In our experiments, we reproduce these frameworks on 14 downstream tasks. This is accomplished by using their pre-trained EEG foundation models with our three standard pipeline strategies and the open-sourced hyperparameter settings available in their online repositories.

B.3 Evaluation Partition

For most datasets, we partition the data using a subject-level split. A subject-dependent strategy is adopted for the SEED

Dataset	Category	#Channel	Duration	#Train	#Valid	#Test	Task
TUAB	Abnormal Classification	23	30	247728	12315	12277	Binary Classification
TUEV	Anomalous Event Detection	21	5	87834	12473	13046	6-class Classification
TUSL	Slowing Event Classification	21,22	10	210	43	37	3-class Classification
SEED	Emotion Recognition	60	10	22455	7875	7560	3-class Classification
SEED-V	Emotion Recognition	60	10	3552	4638	4128	5-class Classification
SEED-VII	Emotion Recognition	60	15	15536	1942	1942	7-class Classification
HMC	Sleep Staging	4	30	91681	22804	22440	5-class Classification
Workload	Mental Stress	19	10	1537	300	297	Binary Classification
Siena	Seizure Detection	29	10	41631	5592	3607	Binary Classification
Mimul-11	Motor Imagery	60	5	31398	5000	4949	3-class Classification
PhysioMI	Motor Imagery	64	4	6210	1734	1803	4-class Classification
BCIC-2a	Motor Imagery	22	4	2784	1152	1152	4-class Classification
Things-EEG-2	Visual Target Detection	63	5	24915	8324	8331	2-class Classification
ADFTD	Alzheimer’s Disease Identification	19	10	4743	1115	1155	3-class Classification

Table 4: Detailed information about evaluation datasets.

and SEED-V datasets to ensure that our metrics are comparable with other baselines. Moreover, we use a greedy, multi-label stratified splitting algorithm to maintain balanced label distributions across the training, validation, and test partitions according to predefined ratios:

- **Siena**: Subject 0-7, 9-13, 16-17 are assigned to the training, validation, test set correspondingly;
- **SEED**: Following prior research, the 15 trials are divided into three sets in a 9:3:3 ratio, and all sessions are merged together thereafter;
- **SEED-V**: Following prior research, the 15 trials are divided into three sets in a 1:1:1 ratio;
- **SEED-VII**: Subjects are randomly split into training, validation, and test sets at a ratio of 8:1:1;
- **PhysioMI**: Subject 1-69,70-88, 89-110 are assigned to the training set, valid set, test set correspondingly;
- **Mimul-11**: Stratified splitting is employed to achieve approximate ratios of 0.76, 0.12, and 0.12 for training, validating, and testing;
- **BCIC-2a**: Subject 1-5,6-7, 8-9 are assigned to the training set, valid set, test set correspondingly;
- **Workload**: Stratified splitting is employed to achieve approximate ratios of 0.72, 0.14, and 0.14 for training, validating, and testing;
- **HMC**: Subjects are randomly split into training, validation, and test sets at a ratio of 103:24:24;
- **TUEV and TUSL**: Owing to the highly imbalanced label distribution in these datasets, the stratified splitting function is employed to create three splits from all the data, approximately aligning with predefined ratios of 0.8, 0.1, and 0.1;
- **TUAB**: The validation and test sets are obtained by equally splitting the original evaluation set by subject, while the training set remains unchanged;
- **Things-EEG-2**: Split by subject with predefined ratios of 0.6, 0.2, and 0.2;

- **ADFTD**: Stratified splitting is employed to achieve approximate ratios of 0.70, 0.15, and 0.15 for training, validating, and testing.

B.4 Evaluation Metrics

To address the class imbalance in downstream datasets, the following evaluation metrics are adopted for comparison:

- **Balanced Accuracy**: the arithmetic mean of recall (sensitivity) across all classes, mitigating the impact of imbalanced class distributions. It is effective for evaluating classification models on datasets with significant disparities in class proportions, which is formulated as:

$$\text{B-Acc} = \frac{1}{C} \sum_{i=1}^C \frac{TP_i}{TP_i + FN_i}, \quad (1)$$

where C is the number of classes, TP_i and FN_i denote true positives and false negatives for class i .

- **Weighted F1**: a harmonic mean of precision and recall, weighted by the number of true instances in each class. This metric accounts for class imbalance by assigning higher importance to classes with larger sample sizes, ensuring a more representative evaluation of model effectiveness, which can be formulated as

$$\text{Pre}_i = \frac{TP_i}{TP_i + FP_i}, \quad \text{Rec}_i = \frac{TP_i}{TP_i + FN_i}, \quad (2)$$

$$\text{W-F1} = \sum_{i=1}^C w_i \cdot \frac{2 \cdot \text{Pre}_i \cdot \text{Rec}_i}{\text{Pre}_i + \text{Rec}_i}, \quad (3)$$

where FP_i denotes false positives for class i , and w_i is the weight of class i based on its support.

- **AUROC**: area under the ROC curve. It reflects the model’s ability to discriminate between classes across all

possible decision boundaries, which is formulated as

$$\text{TPR} = \frac{TP}{TP + FN}, \quad \text{FPR} = \frac{FP}{FP + TN}, \quad (4)$$

$$\text{AUROC} = \int_0^1 \text{TPR}(f) df, \quad f = \text{FPR}. \quad (5)$$

- **AUC-PR:** area under the precision-recall curve. It provides a holistic evaluation of model performance under class imbalance, which can be formulated as

$$\text{AUC-PR} = \int_0^1 \text{Pre}(r) dr, \quad r = \text{Rec}. \quad (6)$$

- **Cohen’s Kappa:** the agreement level between predicted and true labels by comparing observed and expected frequencies along the diagonal of a confusion matrix. It is particularly suited for multi-class classification scenarios, which can be formulated as

$$\kappa = \frac{p_o - p_e}{1 - p_e}, \quad (7)$$

where p_o is the observed agreement and p_e is the expected agreement.

Among these metrics, AUROC and AUC-PR are used to evaluate binary classification tasks, while Cohen’s Kappa and Weighted F1 are applied to multi-category classification. Together, these metrics provide a robust evaluation framework under class imbalance.

B.5 Training Settings

To facilitate data loading, all samples in the datasets are transformed into an Arrow dataset after pre-processing, thus speeding up distributed computing and leveraging the GPU’s direct data access functionality. All experiments are conducted using Python 3.11.13, PyTorch 2.7.1, and CUDA 12.4 on two A100 GPUs. We enable autonomous mixed precision in the bfloat16 data type to improve GPU memory utilization and introduce `GradScaler` to prevent gradient explosion. We employ the AdamW and a two-phase learning rate scheduler, which combines linear warm-up with cosine annealing. The warm-up learning rate factor is set to 0.01. The total training duration is 50 epochs, including 5 warm-up epochs. The gradient clipping value is 1.0. However, for EEGPT, we adopt the OneCycle scheduler according to the original paper. During the downstream classification fine-tuning, the maximum learning rate is set to the corresponding open-sourced implementations. Weight decay is set to 0.01 except CBraMod for 0.05 to enhance the regularization. Batch size is 128. All of the models are fine-tuned in three fine-tuning strategies. We also adopted a differential-learning-rate strategy, configuring the backbone’s learning rate to one-tenth of that assigned to the classifier. The final model for each task is selected based on its validation set performance, with results reported on the held-out test set.

B.6 Model Configurations

Adapter Because several pre-trained architectures were optimized for a fixed set of EEG channels, they cannot

directly accommodate the complete montage used in our pipeline. We therefore applied model-specific adaptation strategies:

- **BENDR and BIOT:** A dynamic-routing convolutional block was inserted ahead of the backbone. This block employs several *Conv1dwithConstraint* layers that project the input recordings onto the channel configuration expected by the pre-trained weights, thereby harmonizing mismatched channel counts.
- **EEGPT:** As EEGPT already covers almost all electrodes in the ‘EasyCap-M1’ montage provided by MNE, performance loss due to the slightly sparser 10-10 layout is negligible. We thus implemented an Adapter that simply removes the electrodes unsupported by the model.
- **LaBraM and CBraMod:** For these models, the original spatial channel layout was flattened into a one-dimensional ordering compatible with their input format.

These adaptations allow each model to ingest the full breadth of our dataset while preserving compatibility with their pre-trained parameters.

Classifier To maintain consistency across every model and dataset combination, we first apply global average pooling over the spatial and temporal dimensions, and then attach a classifier head implemented as a multilayer perceptron with a hidden layer size of 128. This design enables the unified pipeline to accommodate outputs of varying shapes.

C Extended Results

This section presents the complete quantitative results for the seven datasets not included in the main text due to space limitations: TUSL, Mimul-11, Things-EEG-2, SEED-V, ADFTD, BCIC-2a, and SEED-VII. The analysis follows the three fine-tuning strategies outlined in the main text to provide a comprehensive view of model performance.

C.1 Frozen Backbone Single-Task Fine-tuning

The results for the frozen backbone strategy are detailed in Table 5. Consistent with the findings in the main text, we observe a significant performance collapse across nearly all models and datasets. For all remaining 7 tasks, models like BENDR, LaBraM, and CBraMod perform at or very near the level of random chance. For example, on the Mimul-11 dataset, BENDR and CBraMod achieve a Balanced Accuracy of only 33.33 ± 0.00 and 33.34 ± 0.01 , respectively. This confirms the critical “generalization gap” discussed in the main text, showing that representations learned via masked signal reconstruction are not inherently separable or directly applicable to downstream tasks without fine-tuning. While BIOT and EEGPT show marginally better performance on a few tasks (e.g., BIOT achieves 55.69 ± 1.53 B-Acc on TUSL), the overall results underscore the limited “out-of-the-box” utility of foundation models as feature extractors.

C.2 Full-Parameter Single-Task Fine-tuning

Table 6 details the performance under the full-parameter single-task fine-tuning protocol, which assesses each model’s ability to adapt to new tasks. The results continue

to show a varied landscape, with no single model dominating across all seven datasets. CBraMod demonstrates strong performance on tasks requiring fine-grained spatio-temporal analysis, such as TUSL (B-Acc: 67.53 ± 2.16) and Mimul-11 (B-Acc: 51.06 ± 1.27), which aligns with its use of criss-cross attention to model spatial and temporal features separately. EEGPT performs well on the BCIC-2a (B-Acc: 44.07 ± 3.27) and the complex multi-class SEED-V emotion task (B-Acc: 36.43 ± 1.33), suggesting its dual pre-training objective yields robust representations. LaBraM, because of its extensive pre-training and fixed codebook, delivers moderate results while lagging behind other models. BENDR and BIOT, which rely on more generic transformer architectures, generally underperform the more specialized models, except BENDR achieves the best on Things-EEG-2, highlighting the importance of neuro-informed designs for capturing complex EEG dynamics.

C.3 Full-Parameter Multi-Task Fine-tuning

The results of the multi-task fine-tuning strategy are presented in Table 7. This paradigm tests a model’s ability to leverage knowledge across all 14 benchmark tasks simultaneously. As predicted in the main text, multi-task learning serves as a powerful performance catalyst, especially for models that were less competitive in single-task settings. BENDR shows the most dramatic gains, with its B-Acc on TUSL jumping from 47.22 ± 1.48 (single-task) to 73.35 ± 0.98 (multi-task) and on the challenging ADFTD dataset from 37.16 ± 2.62 to 55.71 ± 3.76 . This provides strong evidence that a shared statistical structure exists across diverse EEG paradigms, which models can exploit to learn more generalizable representations. However, consistent with the main text, we also observe instances of negative transfer. For example, the performance of CBraMod and EEGPT on the Things-EEG-2 visual target detection task decreases in the multi-task setting compared to single-task fine-tuning. This suggests that the unique neural patterns of visual stimulus might conflict with patterns from other tasks during joint training, leading to destructive interference.

C.4 Miscellaneous Results

We observed unexpected performance degradation in certain models with motor imagery tasks, and through additional experiments, we identified that the configuration of our classification head may have contributed to this phenomenon. In our standard implementation, classifier adopts average pooling over spatial and temporal dimensions as mentioned in B.6. CBraMod achieves 35.50 ± 0.58 B-Acc and 14.00 ± 0.77 Cohen’s Kappa on BCIC-2a. However, when we adopt the MLP that applies flatten over spatial, temporal and embedding dimensions and resize the hidden layer to 512, CBraMod achieves 47.02 ± 0.47 B-Acc and 29.36 ± 0.62 Cohen’s Kappa on BCIC-2a. Similar improvement was also observed on PhysioMI, CBraMod achieves 60.24 ± 0.53 B-Acc and 47.64 ± 0.39 Cohen’s Kappa using new classifier against the original result 56.74 ± 0.36 B-Acc and 42.31 ± 0.48 Cohen’s Kappa. This suggests that motor imagery classification may need more refined feature interaction to obtain improved representation. Nevertheless,

to ensure consistency across datasets and isolate the backbone’s performance from potential interference caused by the classification head, we maintained the relatively straightforward average pooling scheme.

D Visualization

To complement the quantitative results, this section provides a qualitative analysis of the feature representations learned by each foundation model. We use t-SNE (Maaten and Hinton 2008) to visualize the feature embeddings and Integrated Gradients (Sundararajan, Taly, and Yan 2017) to infer the neurophysiological basis for model decisions, focusing on the results from the full-parameter multi-task fine-tuning strategy. Additional visualizations are presented for TUEV, SEED-VII, Mimul-11, ADFTD, and HMC datasets.

- **TUEV:** This 6-class classification task involves identifying various epileptiform discharges and artifacts. The t-SNE plots (Figure 3) show that CBraMod and EEGPT produce the most coherent clusters, aligning with their superior B-Acc scores in the main text. In contrast, the embeddings from BENDR and BIOT are heavily overlapped or same category fail to cluster together, reflecting their lower quantitative performance. The Integrated Gradients maps for the top models indicate a focus on temporal and central channels, which is consistent with the typical scalp distribution of spike-wave discharges.
- **SEED-V:** This 5-class emotion task is notoriously difficult. The visualizations reveal that all models struggle to form well-separated clusters, which corresponds to the low B-Acc scores across the board (Figure 4). Nonetheless, EEGPT and LaBraM show emergent structures in their embeddings that are absent in other models. The saliency maps suggest that these models attend to channels over the prefrontal and temporal cortices, regions known to be involved in emotion processing, reaffirming the findings from the main text.
- **Mimul-11:** For this 3-class motor imagery task, the t-SNE (Figure 5) plots for EEGPT and BENDR show the clearest class separation, which is reflected in their higher B-Acc scores relative to other models in the multi-task setting (Table 7). The Integrated Gradients visualizations highlight activity in the central and parietal areas of the scalp, corresponding to the location of the motor and somatosensory cortices that govern upper limb movements.
- **ADFTD:** This task requires discriminating between Alzheimer’s Disease (AD), Frontotemporal Dementia (FTD), and healthy controls (CN). The t-SNE (Figure 6) plots show that BENDR and EEGPT, which performed surprisingly well on this task in the multi-task setting, produces reasonably distinct clusters for the AD and CN classes, though the FTD class remains mixed for BENDR. The saliency maps for the better-performing models indicate a focus on frontal, temporal and parietal channels, which aligns with the known progression of cortical atrophy in Alzheimer’s Disease.
- **HMC:** For this 5-class sleep staging task, the t-SNE visualizations (Figure 7) show that the clusters of EEGPT

Model	Metrics	TUSL	Mimul-11	Things EEG 2	SEED-V	ADFTD	BCIC-2a	SEED-VII
BENDR	B-Acc	33.33±0.00	33.33±0.00	50.00±0.00	20.00±0.00	33.33±0.00	25.00±0.00	14.29±0.00
	F1/AUROC	24.02±0.00	38.52±0.00	50.63±0.33	08.53±0.00	22.79±0.00	08.75±1.09	04.85±0.00
	Kappa/AUCPR	00.00±0.00	00.00±0.00	11.08±0.10	00.00±0.00	00.00±0.00	00.00±0.00	00.00±0.00
BIOT	B-Acc	55.69±1.53	35.29±0.80	50.33±0.03	26.14±0.12	39.10±0.36	28.18±0.43	16.54±0.12
	F1/AUROC	52.39±1.64	44.14±1.24	62.49±0.17	25.10±0.17	40.52±0.57	18.33±2.13	15.42±1.63
	Kappa/AUCPR	30.65±2.76	05.53±1.82	15.15±0.07	08.88±0.20	10.17±0.73	03.99±0.61	03.30±0.74
LaBraM	B-Acc	46.03±3.97	33.33±0.00	50.00±0.00	19.98±0.26	25.09±1.32	24.62±0.90	15.59±1.07
	F1/AUROC	30.58±5.78	38.79±0.00	50.02±0.35	09.58±0.76	23.20±0.78	18.70±0.27	09.00±3.51
	Kappa/AUCPR	12.73±8.08	00.00±0.00	11.25±0.10	00.24±0.16	-17.01±0.65	01.60±1.80	05.96±5.09
EEGPT	B-Acc	43.81±0.14	37.11±1.97	50.00±0.00	30.48±0.73	39.03±2.48	39.06±2.09	24.72±0.32
	F1/AUROC	67.86±0.00	44.95±3.07	59.57±0.42	28.71±1.45	32.02±0.53	33.59±2.00	21.85±2.00
	Kappa/AUCPR	60.48±2.18	10.06±3.66	14.18±0.15	12.90±0.57	07.72±3.37	18.75±2.79	13.35±0.35
CBraMod	B-Acc	33.33±0.00	33.34±0.01	50.00±0.00	20.25±0.01	31.78±0.06	24.77±0.20	16.06±0.05
	F1/AUROC	08.96±0.00	38.53±0.02	49.30±0.07	10.12±0.00	28.89±0.14	23.04±0.07	08.96±0.21
	Kappa/AUCPR	00.00±0.00	00.02±0.03	10.51±0.03	00.39±0.02	02.74±0.17	00.31±0.27	02.37±0.08

Table 5: Performance comparison on 7 BCI tasks under frozen fine-tuning strategy.

Model	Metrics	TUSL	Mimul-11	Things EEG 2	SEED-V	ADFTD	BCIC-2a	SEED-VII
BENDR	B-Acc	47.22±1.48	50.44±2.30	65.09±2.02	20.20±0.13	37.16±2.62	35.21±0.54	17.43±0.60
	F1/AUROC	34.17±2.80	59.09±1.23	83.09±0.69	10.72±1.57	40.38±1.69	33.25±0.57	14.20±0.79
	Kappa/AUCPR	17.88±1.95	36.10±3.49	52.68±0.45	00.21±0.13	07.27±4.67	13.62±0.72	03.98±0.69
BIOT	B-Acc	60.05±4.47	40.55±1.14	51.70±0.33	26.66±0.13	34.95±3.17	28.11±0.60	18.89±0.43
	F1/AUROC	56.83±4.49	49.68±1.29	66.01±1.00	25.85±0.13	36.82±3.14	20.86±0.74	16.84±1.12
	Kappa/AUCPR	37.52±6.77	14.45±2.10	18.71±0.36	09.53±0.08	03.75±3.97	04.07±0.90	05.80±0.48
LaBraM	B-Acc	55.89±2.31	47.80±1.68	53.38±0.39	24.35±0.55	27.25±1.98	29.03±0.82	20.39±0.41
	F1/AUROC	39.50±1.73	57.43±1.27	56.38±1.08	23.64±1.21	28.34±2.05	28.50±1.50	19.55±3.82
	Kappa/AUCPR	24.71±3.27	30.71±3.14	13.65±0.45	05.61±1.13	-14.31±1.76	05.07±0.68	09.42±2.64
EEGPT	B-Acc	52.35±3.20	45.19±1.69	62.08±0.58	36.43±1.33	46.50±2.28	44.07±3.27	26.42±0.55
	F1/AUROC	72.68±2.34	54.66±1.38	75.69±1.02	33.00±1.94	48.77±2.56	38.61±4.23	23.89±1.29
	Kappa/AUCPR	66.57±2.63	23.68±2.30	33.32±1.46	18.52±0.67	21.81±3.72	25.42±4.36	14.05±0.99
CBraMod	B-Acc	67.53±2.16	51.06±1.27	62.40±1.56	28.34±0.17	45.02±4.88	33.71±0.86	23.10±0.93
	F1/AUROC	64.36±2.66	59.86±0.92	77.61±0.32	27.48±0.89	44.20±7.00	28.99±1.35	21.82±2.00
	Kappa/AUCPR	46.74±3.54	36.81±2.73	37.48±0.78	10.55±0.20	18.50±7.76	11.61±1.14	09.70±2.62

Table 6: Performance comparison on 7 BCI tasks under separate fine-tuning strategy.

Model	Metrics	TUSL	Mimul-11	Things EEG 2	SEED-V	ADFTD	BCIC-2a	SEED-VII
BENDR	B-Acc	73.35±0.98	52.55±1.52	63.62±1.38	21.75±0.66	55.71±3.76	34.98±0.25	21.98±0.66
	F1/AUROC	70.90±1.73	59.61±2.80	77.23±0.88	19.94±2.58	56.97±2.75	30.01±2.27	19.31±0.87
	Kappa/AUCPR	56.65±2.55	38.35±4.93	42.29±1.75	02.90±0.68	33.98±4.63	13.31±0.33	09.49±1.03
BIOT	B-Acc	61.24±3.28	40.43±0.63	50.86±0.25	30.54±0.18	44.25±1.34	29.66±0.39	20.91±0.41
	F1/AUROC	57.16±5.59	49.02±0.73	63.01±3.12	30.97±0.26	47.02±1.38	23.61±4.64	19.67±1.46
	Kappa/AUCPR	36.19±6.81	14.63±1.88	16.11±2.22	14.14±0.21	18.77±1.80	05.99±0.45	08.46±0.55
LaBraM	B-Acc	75.86±1.15	45.05±0.66	50.90±0.28	43.26±0.29	50.27±1.74	34.58±1.64	26.13±0.92
	F1/AUROC	72.74±1.33	53.42±1.98	54.16±4.06	43.20±0.81	26.17±3.15	31.24±2.71	24.74±0.57
	Kappa/AUCPR	59.60±1.81	22.60±2.20	13.33±1.32	28.93±0.50	52.36±2.23	12.60±2.00	13.07±0.93
EEGPT	B-Acc	76.12±2.05	50.77±0.61	51.54±0.76	43.07±0.60	52.91±1.57	50.52±0.93	27.78±0.47
	F1/AUROC	84.19±1.04	57.44±1.11	66.64±0.04	42.99±0.54	54.82±1.30	48.40±1.86	25.40±0.12
	Kappa/AUCPR	84.30±1.27	31.16±2.43	20.30±0.65	28.62±0.86	31.14±1.85	32.37±2.50	15.80±1.12
CBraMod	B-Acc	79.56±3.24	42.18±0.70	50.70±0.68	40.56±0.77	51.95±2.84	35.50±0.58	26.05±0.72
	F1/AUROC	76.24±4.45	48.90±1.52	66.79±2.55	41.72±0.72	54.41±3.13	23.97±0.25	25.74±1.22
	Kappa/AUCPR	64.72±5.96	17.95±0.88	19.49±2.43	26.22±0.97	30.06±4.35	14.00±0.77	13.09±0.86

Table 7: Performance comparison on 7 BCI tasks under unified fine-tuning strategy.

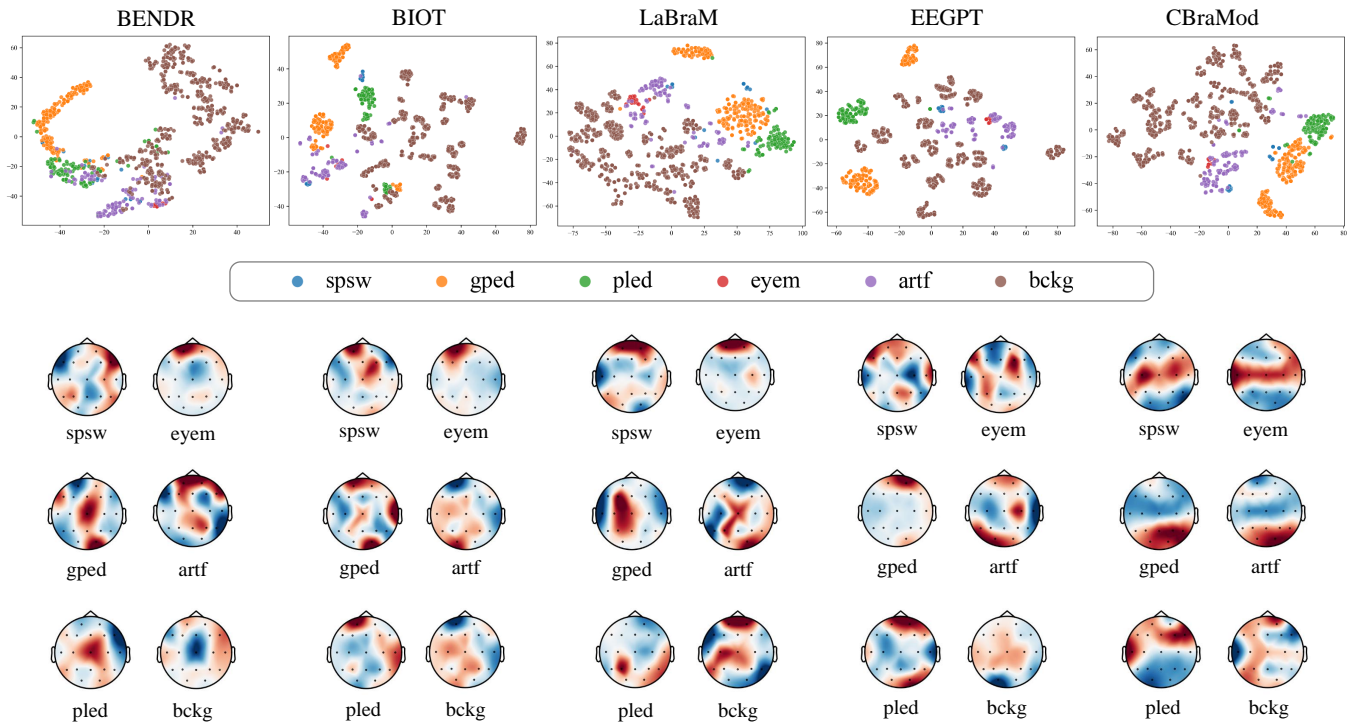


Figure 3: Visualization of models prediction results on TUEV.

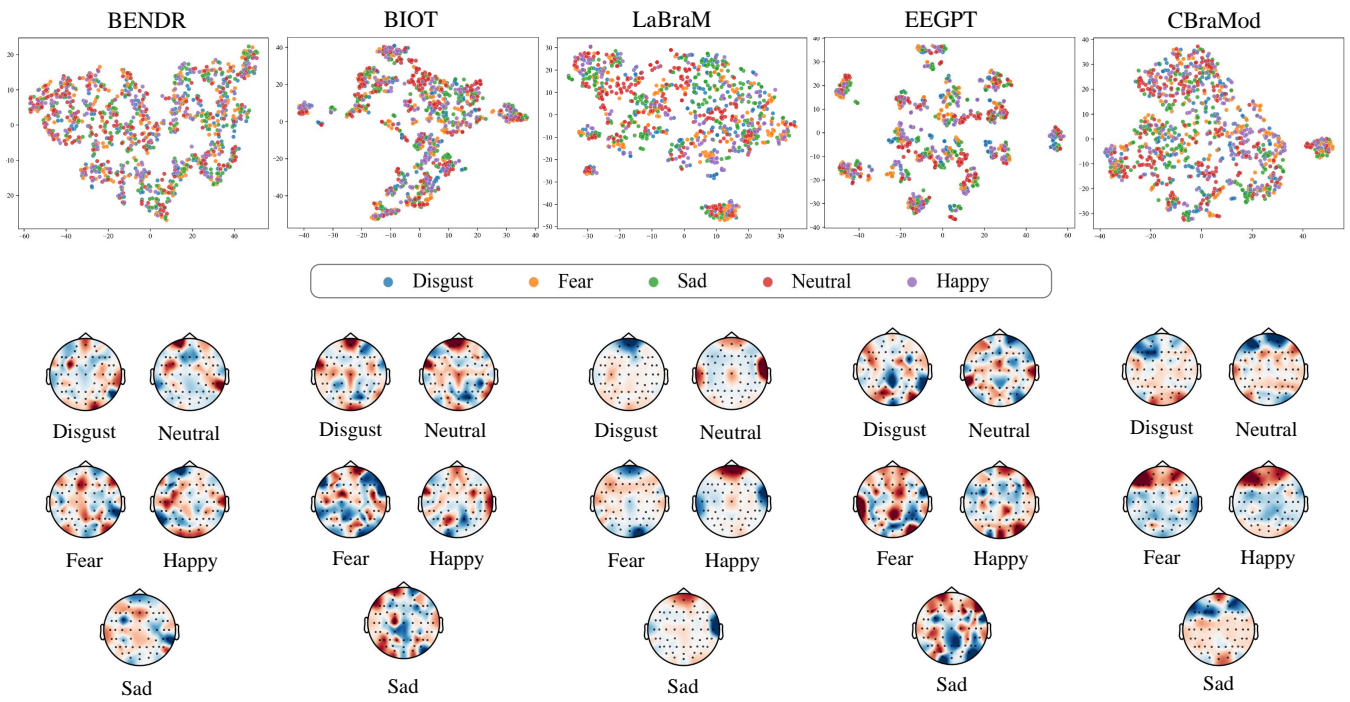


Figure 4: Visualization of models prediction results on SEED-V.

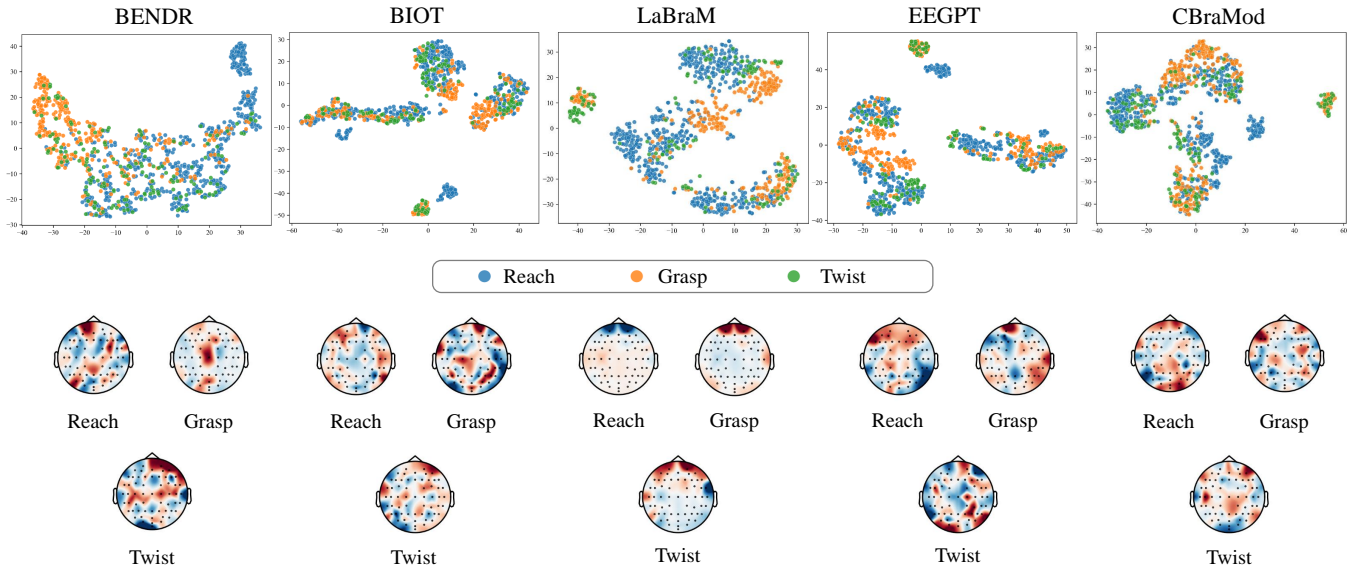


Figure 5: Visualization of models prediction results on Mimul-11.

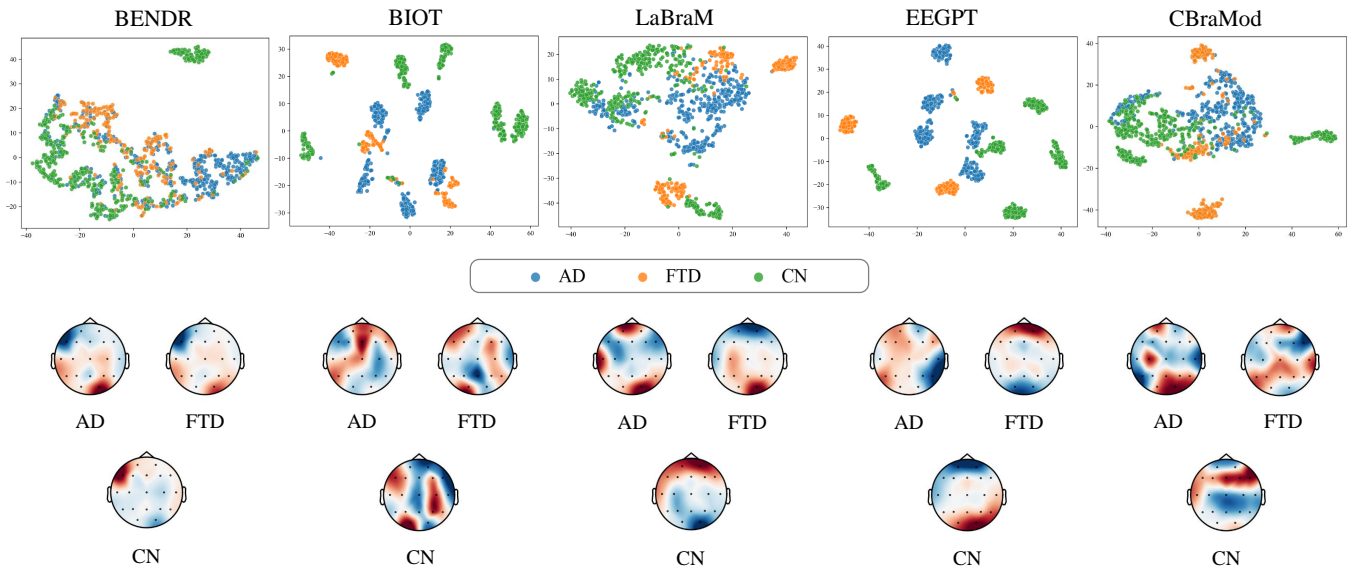


Figure 6: Visualization of models prediction results on ADFTD.

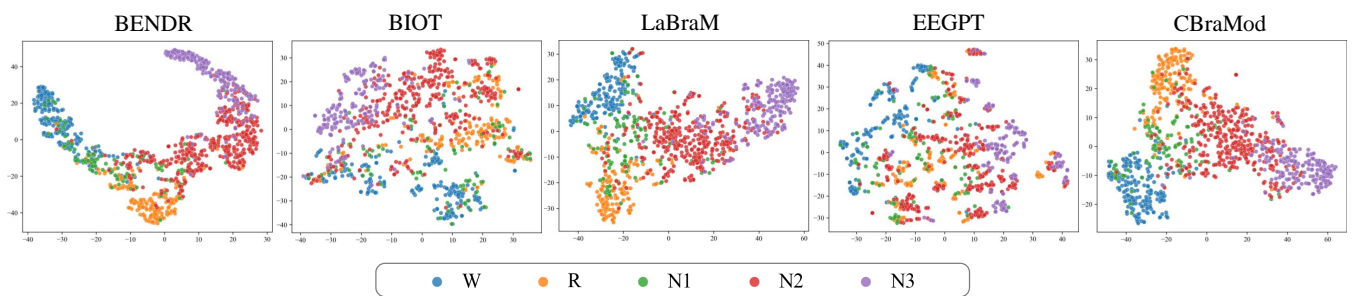


Figure 7: Visualization of models prediction results on HMC.

appear highly fragmented, while CBraMod’s visualization exhibits a radial pattern where the central N2 category overlaps excessively with other categories, which indicates the suboptimal metrics in the table of main text.

E Statistical Significance Analysis

Statistical analysis revealed no significant performance difference between the EEGPT and the CBraMod across the 14 benchmark datasets under separated fine-tuning configuration. A paired samples t-test conducted on the accuracy differences yielded a non-significant result ($t(13) = -0.124, p = 0.548$). The mean accuracy difference was negligible ($\Delta = -0.0024, 95\%CI[-0.0397, 0.0350]$), with the confidence interval spanning zero. The small effect size (Cohen’s $d = -0.033$) further confirms the practical equivalence of both approaches. Although directional variations existed across individual datasets (e.g., +10.36% on BCIC-2a vs. -15.18% on TUSL), these differences balanced out at the aggregate level. These results indicate statistical parity in overall performance ($p \geq 0.05$).

F Limitations and Summary

This benchmark represents a significant step towards standardizing the evaluation of EEG foundation models. However, the process of its construction and the results obtained have illuminated several deeper limitations.

F.1 Limitations

Scope of Benchmark While EEG-FM-Bench covers 14 datasets and 10 paradigms, it does not cover the **multimodal spectrum of EEG applications or close-sourced foundation models**. Future iterations can expand the suite of tasks and continuously integrate new state-of-the-art models to ensure the benchmark remains relevant.

Negative Transfer in Multi-Task Learning Our results demonstrate the power of multi-task learning but also highlight the risk of “negative transfer”, where joint training degrades performance on certain tasks like motor imagery and visual stimulus task. The current implementation fine-tunes all tasks with a single optimizer and learning strategy, which may not be ideal for managing the conflicting optimization landscapes of disparate tasks.

F.2 Summary

The appendix provides supplementary information to support the main paper’s findings. It offers detailed descriptions for each of the 14 datasets used in the benchmark, as well as granular specifics of the experimental setup, covering data pre-processing, hyperparameter settings, and model-specific adaptations used to handle different channel configurations. The appendix also contains the complete quantitative performance tables and additional qualitative visualizations for the seven datasets that were omitted from the main text due to space constraints.